Electronic Supplementary Information

A direct arylation approach towards efficient small molecule organic solar cells

Julija Kudrjasova,[ab] Jurgen Kesters,[ac] Pieter Verstappen,[a] Jeroen Brebels,[a] Tim Vangerven,[c] Ilaria Cardinaletti,[c] Jeroen Drijkoningen,[c] Huguette Penxten,[a] Jean Manca,[d] Laurence Lutsen,[b] Dirk Vanderzande[ab] and Wouter Maes[a,b]*

(a) Design & Synthesis of Organic Semiconductors (DSOS), Institute for Materials Research (IMO-IMOMEC), Hasselt University, Universitaire Campus, Agoralaan 1 - Building D, B-3590 Diepenbeek, Belgium

(b) IMEC, IMOMEC, Universitaire Campus, Wetenschapspark 1, B-3590 Diepenbeek, Belgium

(c) Materials Physics Division, Institute for Materials Research (IMO-IMOMEC), Hasselt University, Universitaire Campus, Wetenschapspark 1, B-3590 Diepenbeek, Belgium

(d) X-LaB, Hasselt University, Universitaire Campus, Agoralaan 1 - Building D, B-3590 Diepenbeek, Belgium

Table of contents

1. General experimental methods

1.1. Synthesis and characterization

Unless stated otherwise, all reagents and chemicals were obtained from commercial sources and used without further purification. 5,5'-Dibromo-4,4'-dinonyl-2,2'-bithiazole,[1] 5,8-dibromo-6-fluoro-2,3-diphenylquinoxaline[2] and (*E*)-6,6'-dibromo-1,1'-bis(2-hexyldecyl)-[3,3'-biindolinylidene]-2,2'-dione[3] were synthesized according to procedures reported in the literature. Toluene was dried using an MBraun solvent purification system (model MB-SPS 800) equipped with alumina drying columns. Microwave reactions were carried out in a CEM Discovery microwave at the given temperature by varying the irradiation power. A thick-wall pyrex reaction vessel (10 mL) with teflon septum was used for the microwave reactions. Preparative size exclusion chromatography (prep-SEC) was performed on JAIGEL 1*H* and 2*H* columns attached to an LC system equipped with a UV detector (path 0.5 mm) and a switch for recycling and collecting the eluent ($CHCl_3$: flow rate 3.5 mL min^{-1}, injection volume 2.5 mL).

NMR chemical shifts (δ) were determined relative to the residual $CHCl_3$ absorption (7.26 ppm) or the ^{13}C resonance shift of $CDCl_3$ (77.16 ppm). MALDI-TOF mass spectra were recorded on a Bruker Daltonics Ultraflex II Tof/Tof. 1 µL of the matrix solution (4 mg mL^{-1} DTCB (*trans*-2-[3-(4-*tert*-butylphenyl)-2-methyl-2-propenylidene]malononitrile) in $CHCl_3$) was spotted onto an MTP Anchorchip 600/384 MALDI plate. The spot was allowed to dry and 1 µL of the analyte solution (0.5 mg mL^{-1} in $CHCl_3$) was spotted on top of the dry matrix. Reported masses originate from the 100% intensity peaks of the isotopic distributions. Rapid heat-cool calorimetry (RHC) experiments were performed on a prototype RHC of TA Instruments, equipped with liquid nitrogen cooling and specifically designed for operation at high scanning rates.[4] RHC measurements were performed at 500 K min^{-1} (after cooling at 20 K min^{-1}; the second heating was chosen to avoid thermal history effects) in aluminum crucibles, using helium (6 mL min^{-1}) as a purge gas. UV-Vis absorption spectra were recorded with an Agilent Cary 500 Scan UV-Vis-NIR spectrometer in a continuous run from 200 to 800 nm at a scan rate of 600 nm min^{-1}. The thin films for the solid-state UV-Vis measurements were prepared by drop casting chloroform solutions of **SM1–3**. To estimate the optical HOMO-LUMO gaps, the wavelength at the intersection of the tangent line drawn at the low energy side of the (solution/film) absorption spectra with the x-axis was used (E_g [eV] = 1240/[wavelength in nm]). Electrochemical measurements were performed with an Eco Chemie Autolab PGSTAT 30 potentiostat/galvanostat using a three-electrode microcell equipped with a Pt wire working

electrode, a Pt wire counter electrode and a $Ag/AgNO_3$ reference electrode (Ag wire dipped in a solution of 0.01 M $AgNO_3$ and 0.1 M NBu_4PF_6 in anhydrous MeCN). Samples were prepared in anhydrous CH_2Cl_2 (MeCN for films) containing 0.1 M NBu_4PF_6, and ferrocene was used as a reference. The respective small molecules were dissolved in the electrolyte solution, which was degassed with Ar prior to each measurement. To prevent air from entering the system, the experiments were carried out under a curtain of Ar. Cyclic voltammograms were recorded at a scan rate of 50 mV s^{-1}. The HOMO-LUMO energy levels of the products were estimated from the obtained CV data. For the conversion of V to eV, the onset potentials of the first oxidation/reduction peaks were used and referenced to ferrocene/ferrocenium, which has an ionization potential of −4.98 eV *vs.* vacuum. This correction factor is based on a value of 0.31 eV for Fc/Fc^+ *vs.* SCE[5a] and a value of 4.68 eV for SCE *vs.* vacuum[5b]: $E_{HOMO/LUMO}$ (eV) = −4.98 − $E_{onset\ ox/red}{}^{Ag/AgNO3}$ (V) + $E_{onset\ Fc/Fc+}{}^{Ag/AgNO3}$ (V). The accuracy of measuring redox potentials by CV is about 0.01−0.02 V. Reproducibility can be less because the potentials do depend on concentration and temperature.[6]

(TPA-T-TzTz-T)$_2$BiTz (SM1). 4-{4-Hexyl-5-[5-(3-hexylthiophen-2-yl)thiazolo[5,4-*d*]thiazol-2-yl]thiophen-2-yl}-*N*,*N*-diphenylaniline (**TPA-T-TzTz-T**) (100 mg, 0.14 mmol, 2 equiv), K_2CO_3 (28.9 mg, 0.209 mmol, 3 equiv), $Pd(OAc)_2$ (0.6 mg, 2.8 µmol, 4 mol%), PCy_3HBF_4 (2.0 mg, 5.6 µmol, 8 mol%), pivalic acid (4.3 mg, 0.075 mmol) and 5,5'-dibromo-4,4'-dinonyl-2,2'-bithiazole (40.3 mg, 0.07 mmol, 1 equiv) were weighed in air and placed in a microwave vial (10 mL) equipped with a magnetic stirring bar. The vial was purged with Ar and dry toluene (2 mL) was added. The reaction mixture was vigorously stirred under microwave irradiation at 150 °C for 18 h. The solution was then cooled down to room temperature and diluted with CH_2Cl_2 and H_2O. The aqueous phase was extracted with CH_2Cl_2. The organic fractions were combined and dried over $MgSO_4$, filtered, and evaporated under reduced pressure. The obtained product mixture was separated by column chromatography on silica gel using a mixture of CH_2Cl_2 and petroleum ether (2/3) as the eluent. The fractions containing the desired product (with minor impurities) were collected and the small molecule was additionally purified by recycling prep-SEC to afford **SM1** as a pure dark red solid (42 mg, 33%). ^{1}H NMR (400 MHz, $CDCl_3$) δ = 7.44 (d, J = 8.6 Hz, 4H), 7.30–7.27 (m, 6H), 7.25–7.24 (m, 2H), 7.14–6.97 (m, 20H), 2.98 (t, J = 7.8 Hz, 4H), 2.95–2.84 (m, 8H), 1.85 (p, J = 7.6 Hz, 4H), 1.82–1.66 (m, 8H), 1.54–1.42 (m, 12H), 1.43–1.22 (m, 36H), 0.97–0.84 (m, 18H); ^{13}C NMR (75 MHz, $CDCl_3$) δ = 161.6, 160.1, 157.4, 155.3, 150.4, 150.1, 148.1, 147.4, 145.7, 144.3, 143.1, 134.5, 132.6, 130.5, 130.2, 129.5, 127.9, 127.2, 126.6, 125.7,

125.0, 123.6, 123.1, 32.1, 31.9, 31.0, 30.8, 30.5, 29.8, 29.6, 29.3, 22.8, 14.3; MS (MALDI-TOF) calcd. for $C_{108}H_{122}N_8S_{10}$ *m/z* = 1851.7 ([M]$^+$), found *m/z* = 1853.0; UV-Vis ($CHCl_3$) λ_{max} (log ε) = 492 nm (4.704).

(TPA-T-TzTz-T)$_2$Qx (SM2). Precursor **TPA-T-TzTz-T** (100 mg, 0.14 mmol, 2 equiv), K_2CO_3 (28.9 mg, 0.209 mmol, 3 equiv), $Pd(OAc)_2$ (0.6 mg, 2.8 µmol, 4 mol%), PCy_3HBF_4 (2.0 mg, 5.6 µmol, 8 mol%), pivalic acid (4.3 mg, 0.075 mmol) and 5,8-dibromo-6-fluoro-2,3-diphenylquinoxaline (31.9 mg, 0.07 mmol, 1 equiv) were weighed in air and placed in a microwave vial (10 mL) equipped with a magnetic stirring bar. The vial was purged with Ar and dry toluene (2 mL) was added. The reaction mixture was vigorously stirred under microwave irradiation at 150 °C for 18 h. The solution was then cooled down to room temperature and diluted with CH_2Cl_2 and H_2O. The aqueous phase was extracted with CH_2Cl_2. The organic fractions were combined and dried over $MgSO_4$, filtered, and evaporated under reduced pressure. The obtained product mixture was separated by column chromatography on silica gel using a mixture of $CHCl_3$ and petroleum ether (1/1) as the eluent to afford **SM2**. Minor remaining impurities were removed by precipitating the small molecule (twice) from EtOAc. The pure product was obtained as a dark purple solid (35 mg, 29%). Due to its limited solubility in $CHCl_3$, the product could not be further purified by recycling prep-SEC. ^{1}H NMR (300 MHz, $CDCl_3$) δ = 7.78–7.58 (m, 5H), 7.52–7.34 (m, 12H), 7.33–7.26 (m, 6H), 7.25–7.21 (m, 2H), 7.17–6.83 (m, 18H), 3.07–2.52 (m, 8H), 1.80–1.62 (m, 8H), 1.53–1.28 (m, 24H), 1.02–0.86 (m, 12H); MS (MALDI-TOF) calcd. for $C_{104}H_{95}FN_8S_8$ *m/z* = 1731.5 ([M]$^+$), found *m/z* = 1731.5; UV-Vis ($CHCl_3$) λ_{max} (log ε) = 527 (4.79), 437 nm (4.78). Due to the compound's limited solubility, ^{13}C NMR data were not gathered.

(TPA-T-TzTz-T)$_2$II (SM3). Precursor **TPA-T-TzTz-T** (100 mg, 0.14 mmol, 2 equiv), K_2CO_3 (28.9 mg, 0.209 mmol, 3 equiv), $Pd(OAc)_2$ (0.6 mg, 2.8 µmol, 4 mol%), PCy_3HBF_4 (2.0 mg, 5.6 µmol, 8 mol%), pivalic acid (4.3 mg, 0.075 mmol) and 6,6'-dibromo-1,1'-bis(2-hexyldecyl)-[3,3'-biindolinylidene]-2,2'-dione (49.5 mg, 0.07 mmol, 1 equiv) were weighed in air and placed in a microwave vial (10 mL) equipped with a magnetic stirring bar. The vial was purged with Ar and dry toluene (2 mL) was added. The reaction mixture was vigorously stirred under microwave irradiation at 150 °C for 18 h. The solution was then cooled down to room temperature and diluted with CH_2Cl_2 and H_2O. The aqueous phase was extracted with CH_2Cl_2. The organic fractions were combined and dried over $MgSO_4$, filtered, and evaporated under reduced pressure. The obtained product mixture was separated by column chromatography on silica gel using a mixture of CH_2Cl_2 and petroleum ether (1/2). The fractions

containing the desired product (with minor impurities) were collected and the small molecule was additionally purified by recycling prep-SEC to afford **SM3** as a black solid (47 mg, 32%). ^{1}H NMR (300 MHz, $CDCl_3$) δ = 9.10 (d, J = 8.5 Hz, 2H), 7.43 (d, J = 8.7 Hz, 4H), 7.32–7.27 (m, 6H), 7.25–7.24 (m, 2H), 7.22–6.97 (m, 22H), 6.81 (s, 2H), 3.76–3.62 (m, 4H), 2.98–2.78 (m, 8H), 1.92 (s_{br}, 2H), 1.81–1.65 (m, 8H), 1.44–1.12 (m, 70H), 1.02–0.90 (m, 12H), 0.89–0.78 (m, 12H); ^{13}C NMR (75 MHz, CD_2Cl_2) δ = 168.9, 161.5, 160.7, 150.8, 148.5, 148.0, 146.0, 145.7, 145.0, 144.6, 144.2, 136.1, 132.9, 131.5, 131.2, 131.1, 130.1, 127.7, 127.4, 127.0, 126.0, 125.7, 124.2, 123.4, 122.2, 118.5, 104.5, 45.1, 37.5, 32.8, 32.6, 31.5, 31.1, 30.8, 30.6, 30.4, 30.3, 27.6, 23.7, 23.6, 14.8.; MS (MALDI-TOF) calcd. for $C_{132}H_{156}N_8O_2S_8$ m/z = 2142.0 ($[M]^+$), found m/z = 2142.5; UV-Vis ($CHCl_3$) λ_{max} (log ε) = 598 (4.99), 449 nm (5.02).

1.2. Photovoltaic device fabrication and characterization

Bulk heterojunction organic solar cells were fabricated using the traditional device architecture glass/ITO/PEDOT:PSS/photoactive layer/Ca/Al. Prior to processing, the pre-patterned indium tin oxide (ITO, Kintec, 100 nm, 20 Ohm/sq) coated glass substrates were thoroughly cleaned using soap, demineralized water, acetone, isopropanol and a UV/O_3 treatment. PEDOT:PSS [poly(3,4-ethylenedioxythiophene):poly(styrenesulfonic acid), Heraeus Clevios] was deposited by spin-coating, aiming at a layer thickness of ~30 nm. Afterwards, processing was continued under nitrogen atmosphere in a glove box (<1 ppm O_2/H_2O), starting off with an annealing step at 130 °C for 15 min to remove any residual water. Subsequently, all active layer small molecule:$PC_{71}BM$ ([6,6]-phenyl-C_{71}-butyric acid methyl ester; Solenne, >99%) blend solutions were spin-coated with optimal layer thicknesses of ~120−150 nm, as confirmed by profilometry (DEKTAK). Optimal device performances were procured for the small molecules processed from chloroform-based blends in a 1:1 (wt/wt%) ratio in combination with $PC_{71}BM$ (stirred overnight at 50 °C) and a small molecule concentration of 8 mg mL^{-1}. In a final step, devices with an active area of 3 mm² were obtained by evaporation of Ca and Al as top electrodes, with thicknesses of 30 and 80 nm, respectively. For the device employing the conjugated polyelectrolyte (CPE) cathodic interlayer, Ca was not incorporated in the device stack. Prior to spin-coating on top of the **SM2**:$PC_{71}BM$ photoactive layer, the CPE material was dissolved in methanol with an optimized concentration of 0.6 mg mL^{-1}. The I-V characteristics of the resulting photovoltaic devices were evaluated under AM1.5G solar illumination (100 mW cm^{-2}) using a Newport class A solar simulator

(model 91195A), calibrated with a silicon solar cell. External quantum efficiency (EQE) measurements were performed with a Newport Apex illuminator (100 W Xenon lamp, 6257) as a light source, a Newport Cornerstone 130° monochromator and a Stanford SR530 lock-in amplifier for the current measurements. A silicon FDS100-CAL photodiode was employed as a reference cell. The chopper frequency was set at 24 Hz. For atomic force microscopy (AFM) imaging, a Bruker Multimode 8 AFM was used in PeakForce tapping mode, employing ScanAsyst. The images were produced with a silicon tip on a nitride lever with a spring constant of 4 N m^{-1}. Photo-induced charge extraction by linearly increasing voltage (Photo-CELIV) signals were registered on complete photovoltaic devices utilizing a pulsed laser (Continuum minilite II, 532nm), a Tektronix TDS 620B oscilloscope and a Tektronix AFG3101 function generator. The samples were placed in a sample holder filled with nitrogen to avoid exposure to ambient air. Organic field-effect transistors (OFET's) were prepared in the bottom gate bottom contacts configuration by spin-coating solutions of **SM1−3** in chloroform with a concentration of 4 mg mL^{-1} on 200 nm of SiO_2, thermally grown on a highly n-doped Si substrate with pre-patterned contacts comprising of a stack of Ti/Au (10/100 nm), obtained from Philips. A self-assembled monolayer of HMDS (hexamethyldisilazane) passivated the bare SiO_2 surface. The channel length was 10 µm, while the channel widths ranged between 7.5 and 20 mm (interdigitated electrodes). Two Keithley 2400 source meters were used to measure the current at the drain and correct it for leakage through the gate electrode. All FET preparation and characterization was carried out in a N_2 filled glove box and the mobility values for each compound were averaged over 5 devices. Fourier transform photocurrent spectroscopy (FTPS) was performed using a Thermo Nicolet 8700 FTIR with an external detector. The spectra were recorded with a quartz beamsplitter and appropriate optical bandpass filters to improve the signal to noise ratio. All spectra were corrected for the frequency response. More information on the applied setup can be found in literature.[7]

2. MALDI-TOF mass spectra of small molecules SM1−3

(TPA-T-TzTz-T)$_2$BiTz (**SM1**)

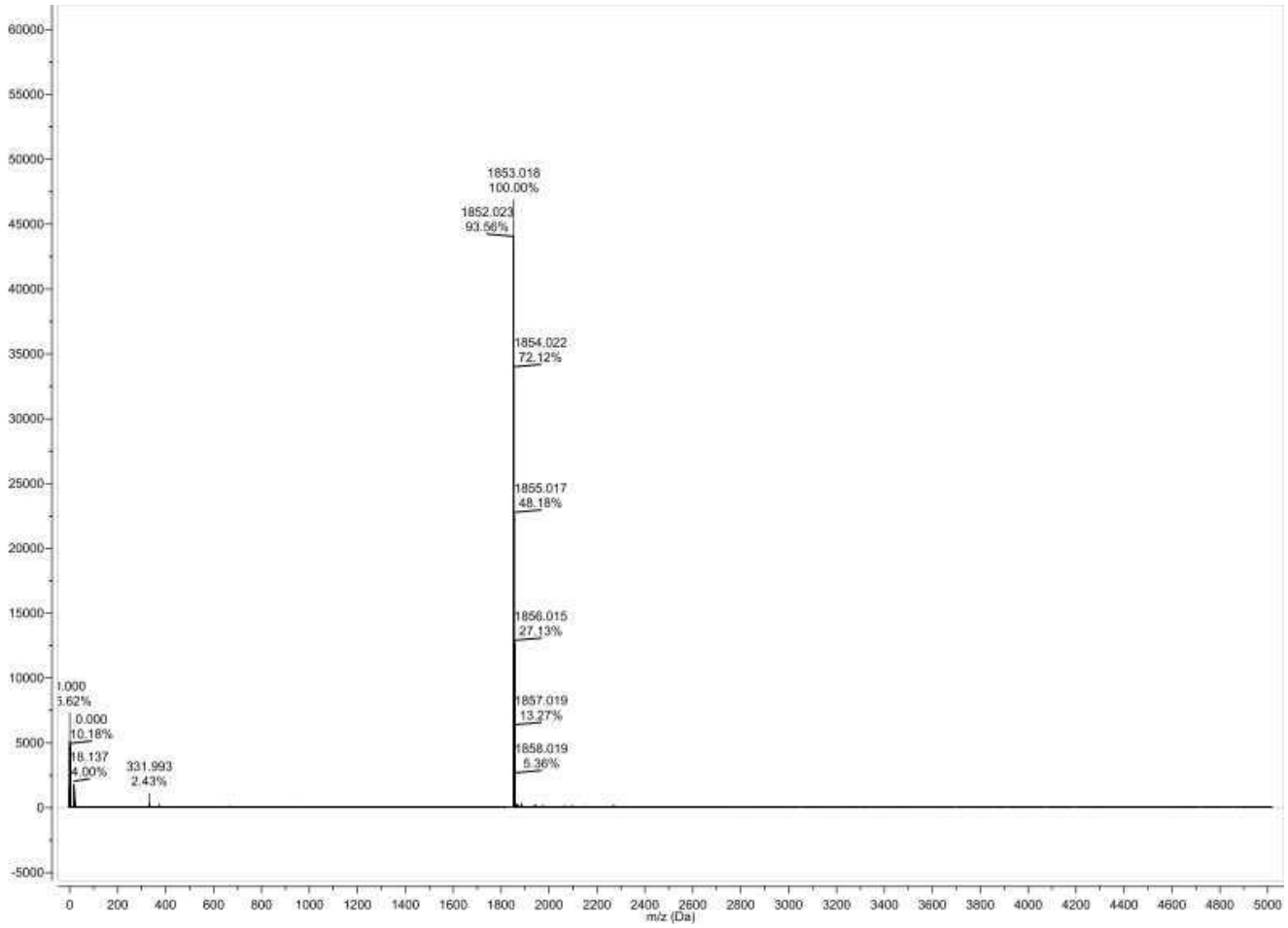

Figure S1. MALDI-TOF mass spectrum of **SM1**.

(TPA-T-TzTz-T)$_2$Qx (**SM2**)

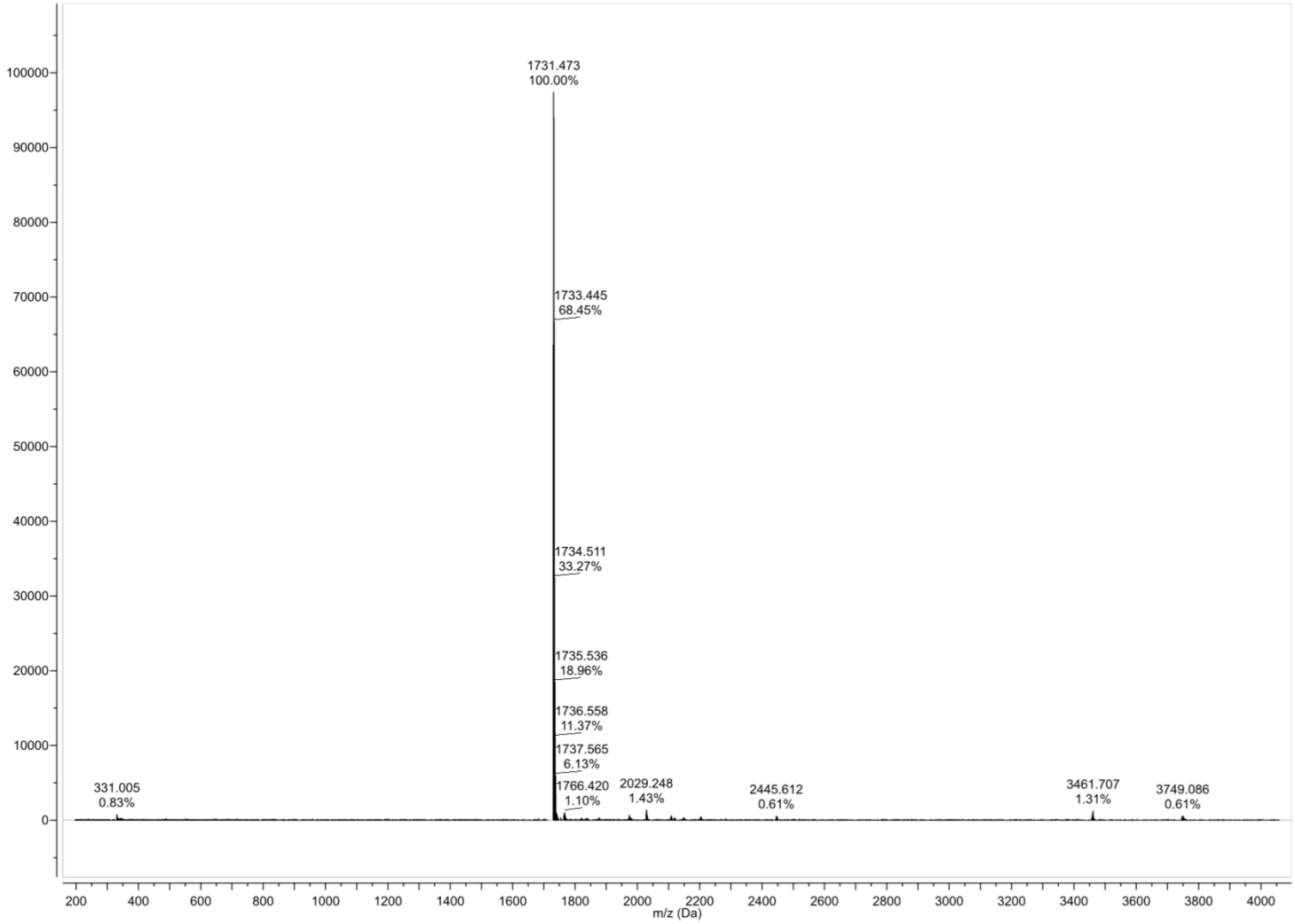

Figure S2. MALDI-TOF mass spectrum of **SM2**.

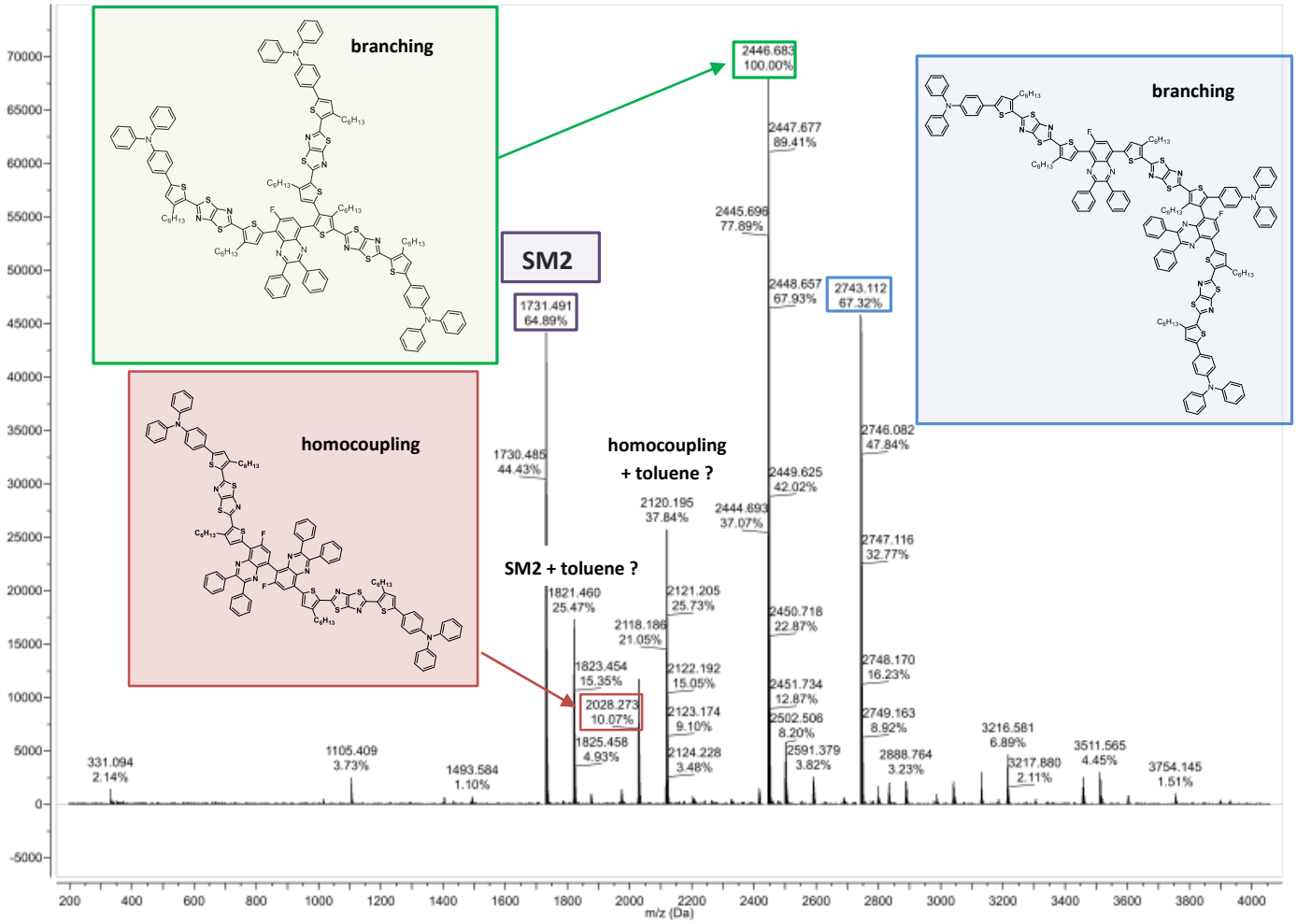

Figure S3. MALDI-TOF mass spectrum of the filtrate after precipitation of **SM2**, illustrating some of the side products formed upon direct (hetero)arylation (the exact position of the branching points and the regioselectivity of the Qx building block remain unknown).

(TPA-T-TzTz-T)$_2$II (**SM3**)

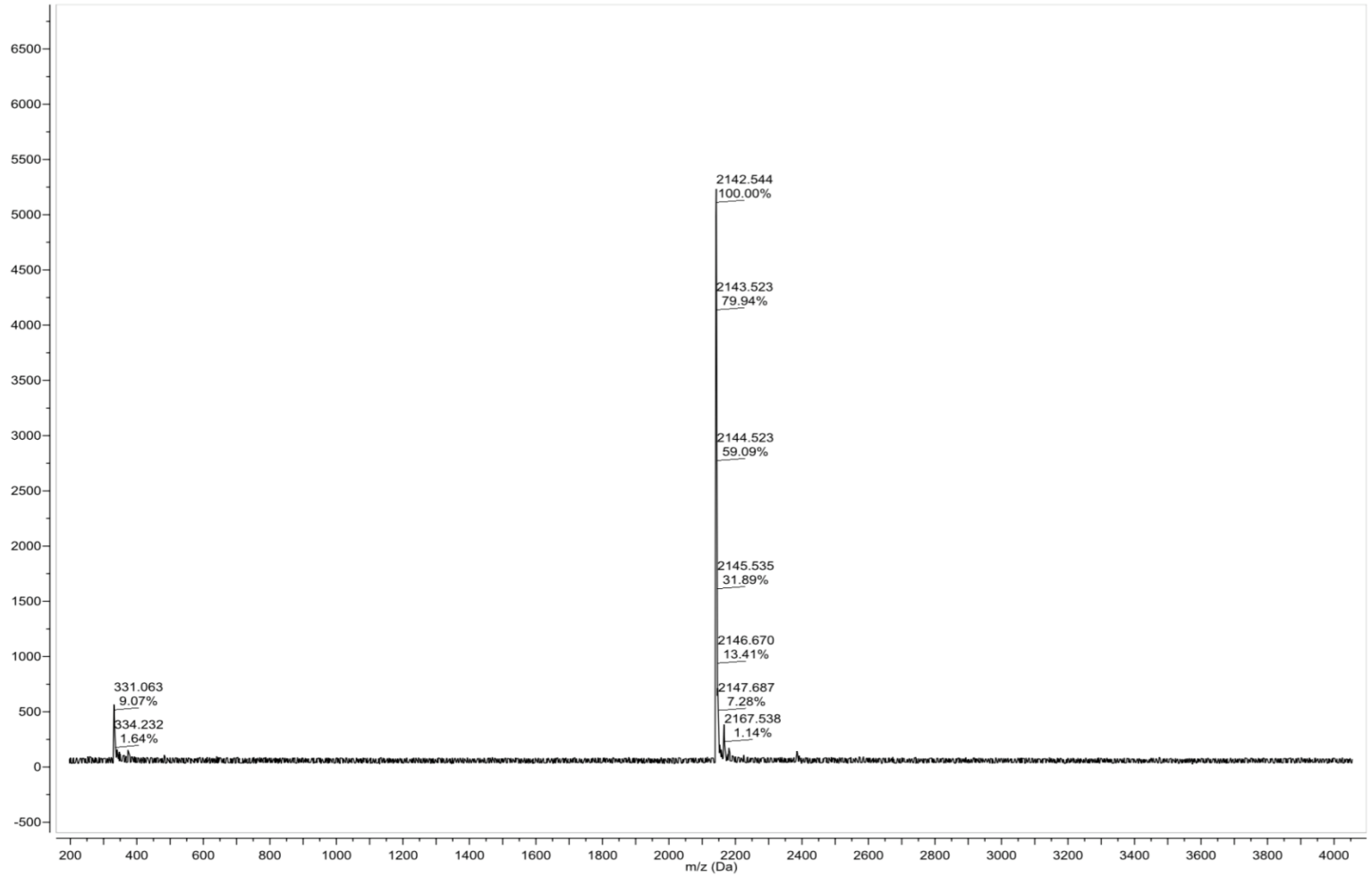

Figure S4. MALDI-TOF mass spectrum of **SM3**.

3. NMR spectra ($^{1}H/^{13}C$) of small molecules SM1–3

(TPA-T-TzTz-T)$_2$BiTz (**SM1**)

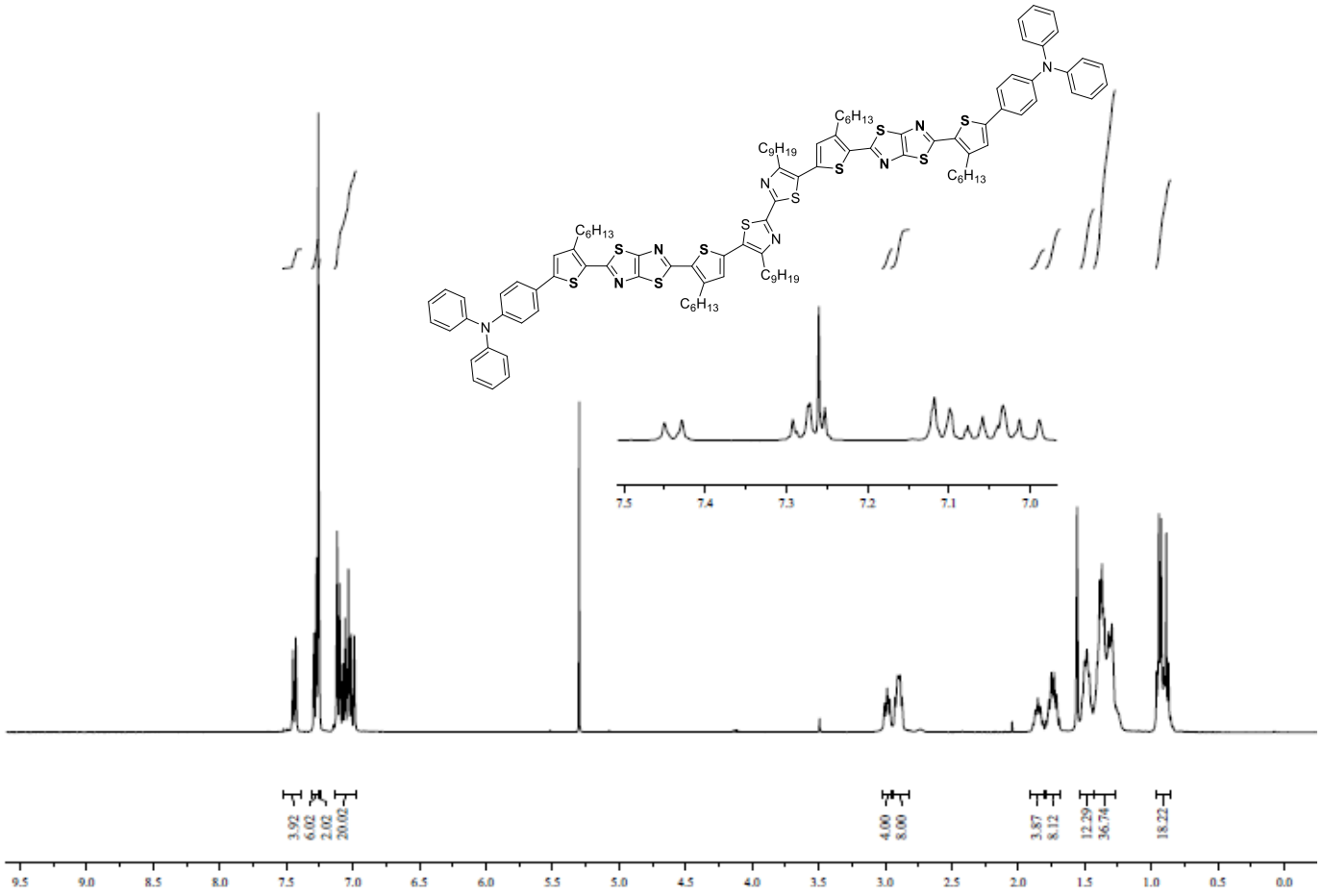

Figure S5. ^{1}H NMR spectrum of **SM1** ($CDCl_3$, 400 MHz).

(TPA-T-TzTz-T)$_2$BiTz (**SM1**)

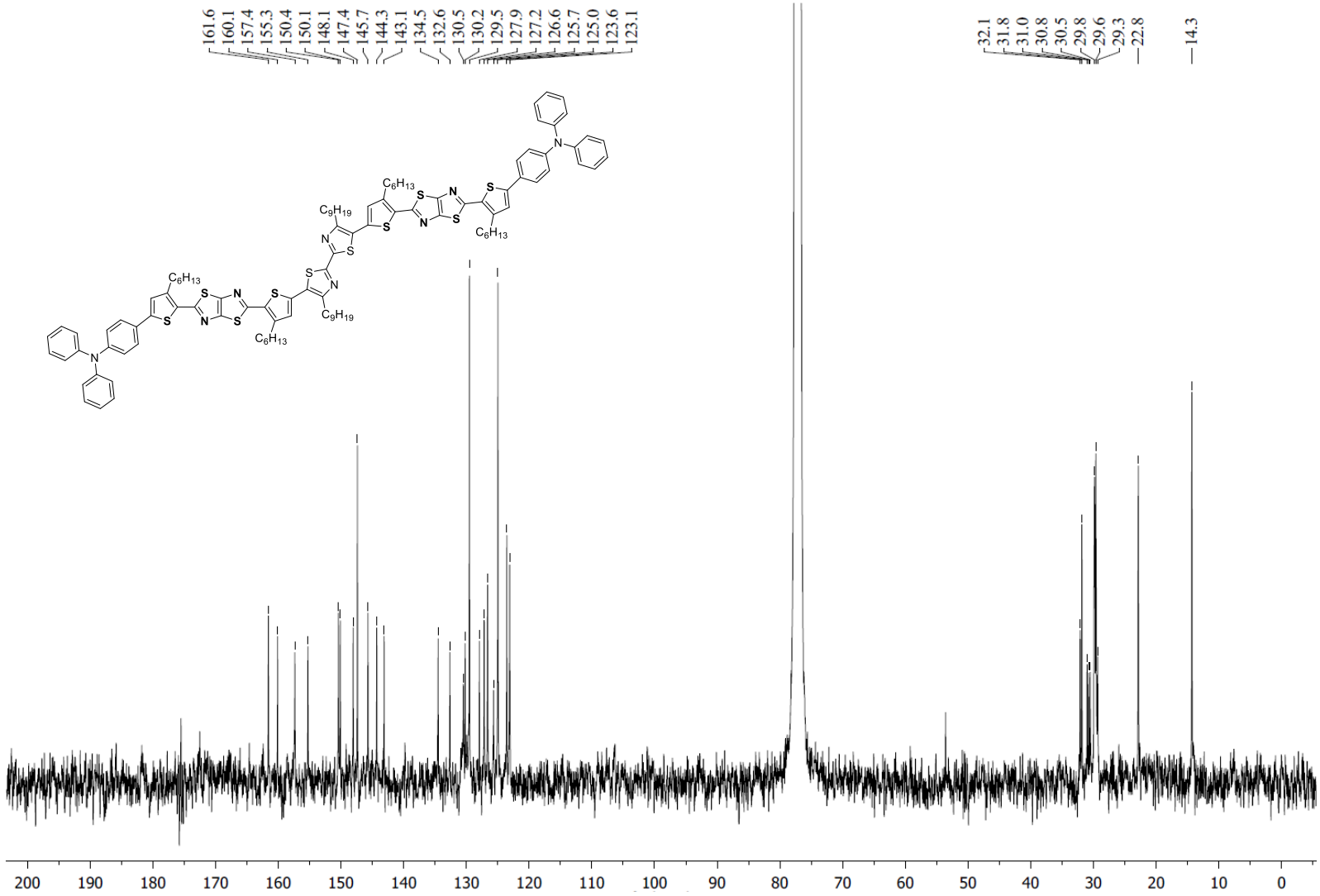

Figure S6. ^{13}C NMR spectrum of **SM1** ($CDCl_3$, 75 MHz).

(TPA-T-TzTz-T)$_2$Qx (**SM2**)

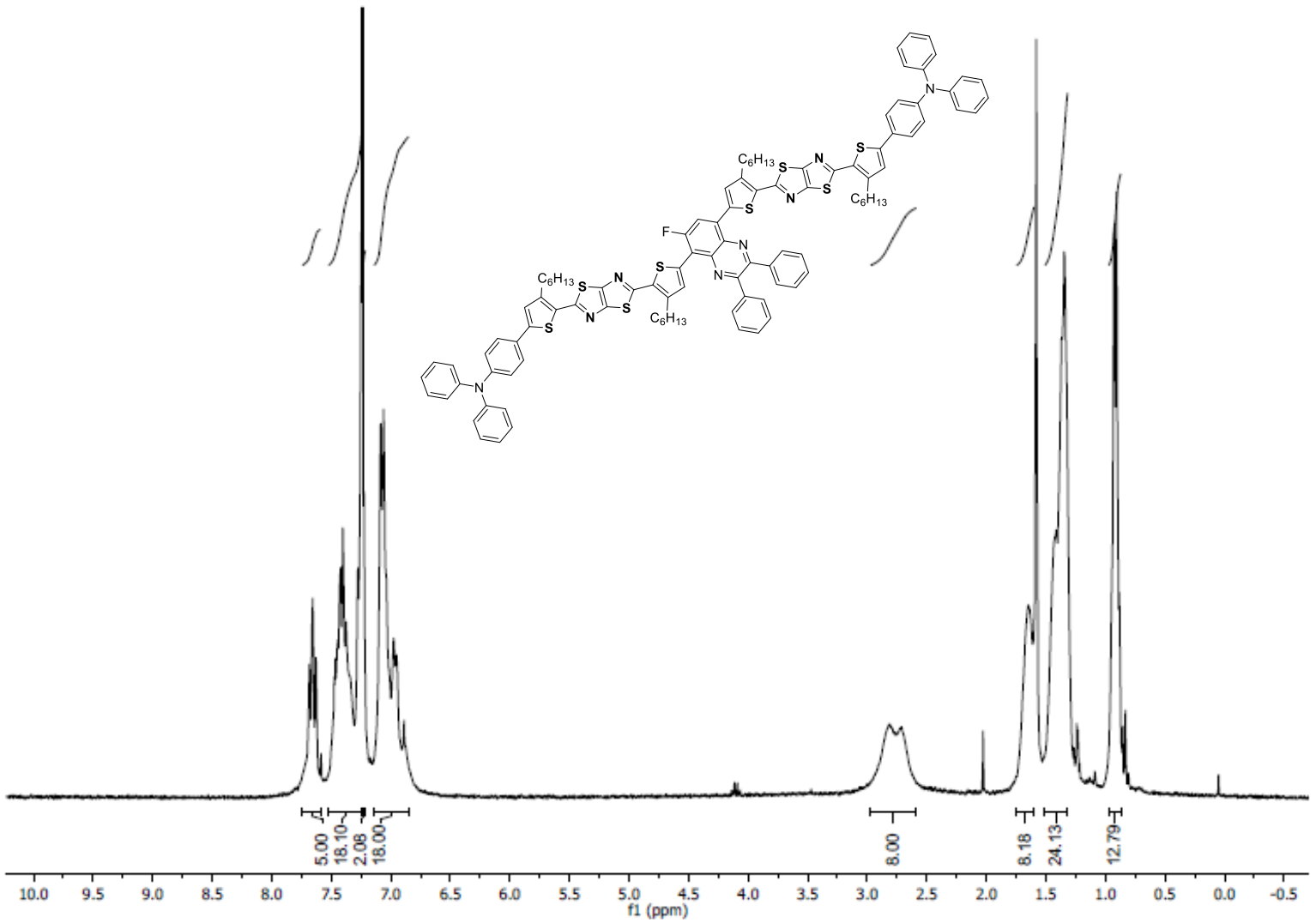

Figure S7. ^{1}H NMR spectrum of **SM2** ($CDCl_3$, 300 MHz).

(TPA-T-TzTz-T)$_2$II (**SM3**)

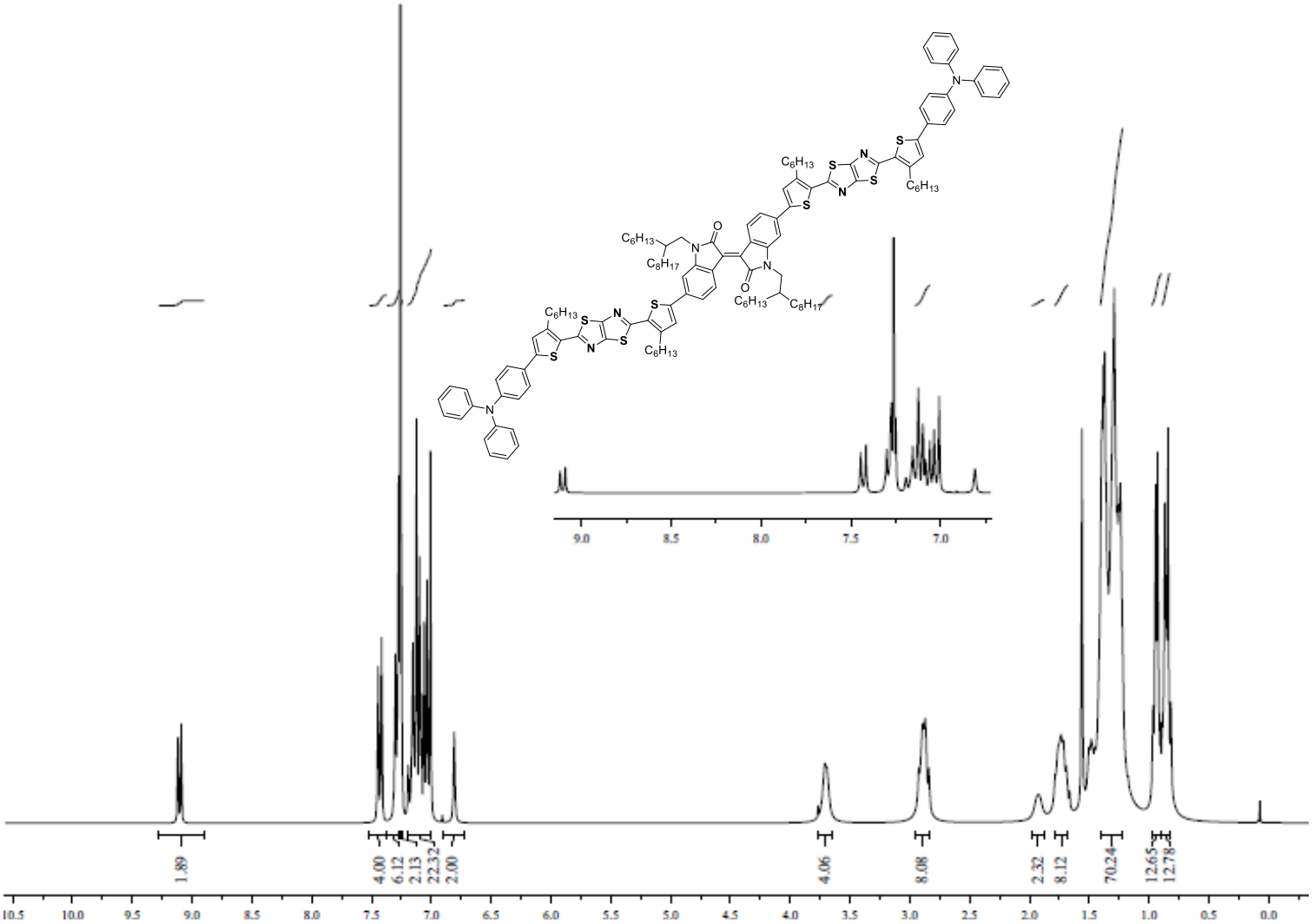

Figure S8. ^{1}H NMR spectrum of **SM3** ($CDCl_3$, 300 MHz).

(TPA-T-TzTz-T)$_2$II (**SM3**)

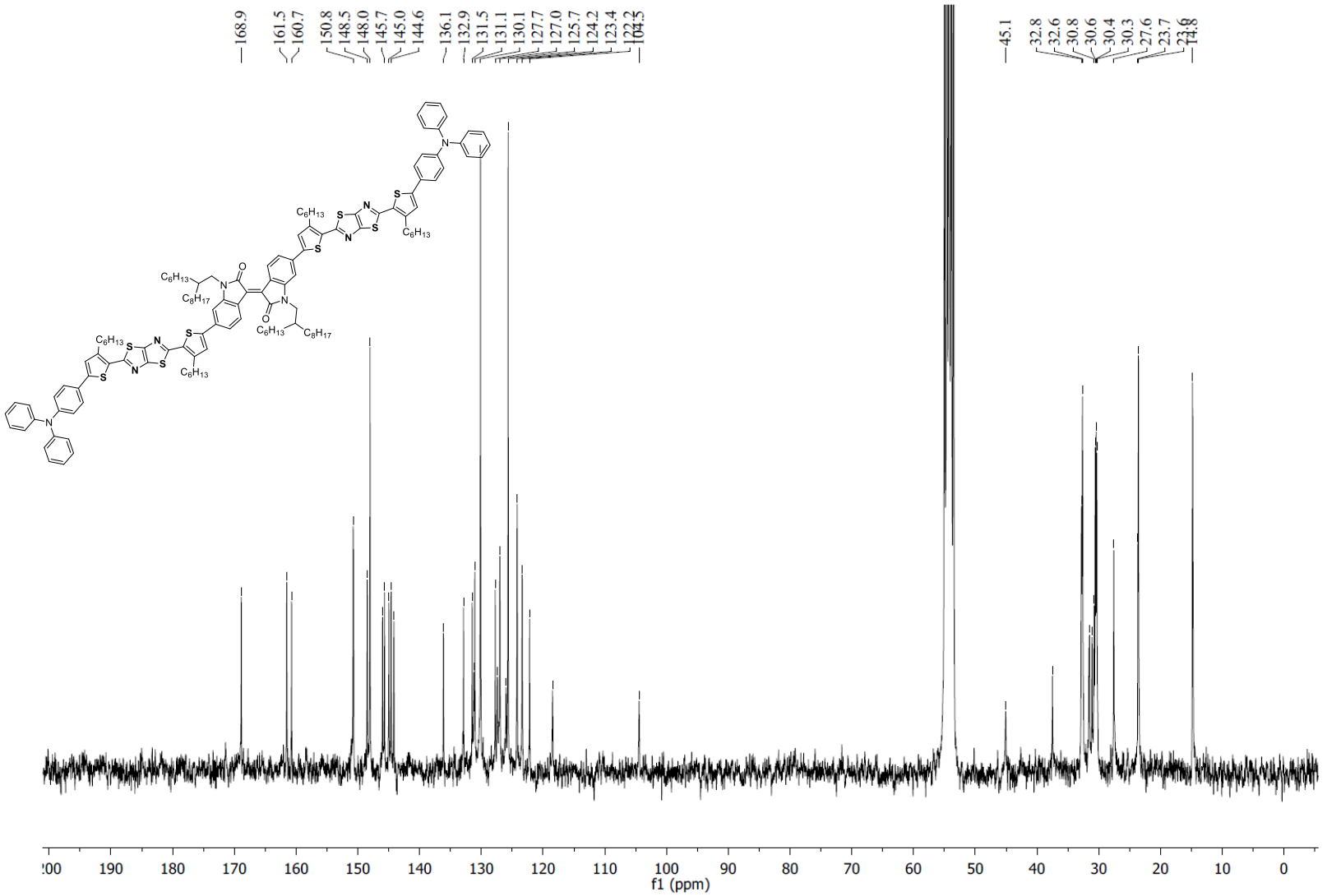

Figure S9. ^{13}C NMR spectrum of **SM3** ($CDCl_3$, 75 MHz).

4. UV-Vis absorption spectra of small molecules SM1−3 (in solution)

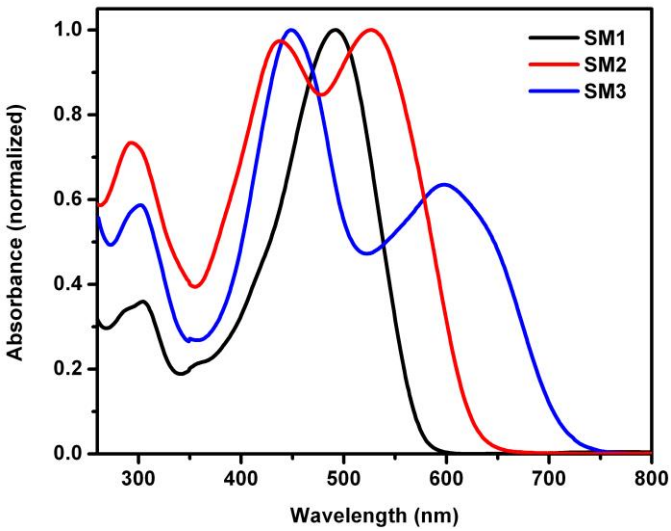

Figure S10. UV-Vis absorption spectra (normalized) of small molecules **SM1−3** in $CHCl_3$ solution.

5. Cyclic voltammograms of small molecules SM1–3

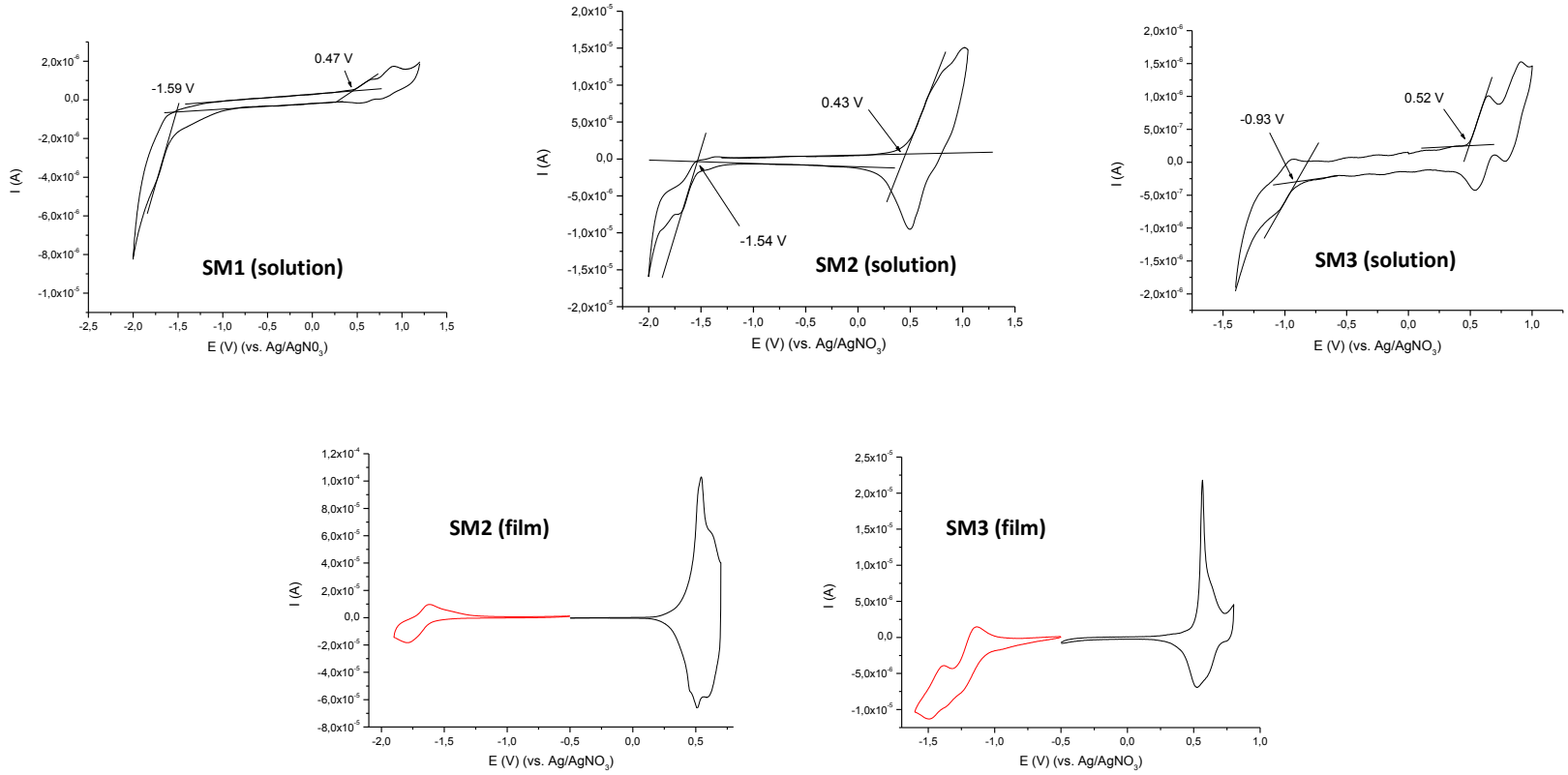

Figure S11. Cyclic voltammograms of small molecules **SM1–3** in solution (upper row) and film (bottom row).

For **SM2** (causing some solubility issues) and **SM3**, the CV measurements were conducted in film as well, providing very similar results (**SM2**: E_{ox}^{onset} = 0.45 V, E_{red}^{onset} = −1.62 V, E_g^{OP} = 1.75 eV; **SM3**: E_{ox}^{onset} = 0.53 V, E_{red}^{onset} = −1.06 V, E_g^{OP} = 1.61 eV; Fig. S11).

6. Optimization of the SM1−3:$PC_{71}BM$ organic solar cell performances

Table S1. Optimization of the solar cell devices based on **SM1**.

Processing solvent[a]	**SM1**:$PC_{71}BM$	Total concentration (mg mL^{-1})	V_{OC} (V)	J_{SC} (mA cm^{-2})	FF	Average η (%)[b]	Best η (%)
CF	2:1	15	0.80	3.60	0.60	1.74	1.78
CF	1:1	16	0.75	5.80	0.41	1.77	1.96
CF	1:3	16	0.70	3.31	0.28	0.66	0.93
CF + 1% CN	1:1	16	0.76	6.14	0.54	2.50	2.78
CF + 3% CN	1:1	16	0.79	3.44	0.50	1.35	1.41

[a] CF = chloroform, CN = 1-chloronaphthalene. [b] Average values over at least 4 devices.

Table S2. Optimization of the solar cell devices based on **SM2**.

Processing solvent[a]	**SM2**:$PC_{71}BM$	Total concentration (mg mL^{-1})	V_{OC} (V)	J_{SC} (mA cm^{-2})	FF	Average η (%)[b]	Best η (%)
CF	2:1	15	0.89	6.95	0.43	2.66	2.77
CF	1:1	16	0.84	9.29	0.55	4.25	4.86
CF	1:3	16	0.79	7.12	0.34	1.93	1.92
CF + 1% CN	1:1	16	0.86	7.81	0.40	2.68	2.84
CF + 3% CN	1:1	16	0.84	6.89	0.42	2.43	2.72
CB	1:1	32	0.81	6.60	0.35	1.86	1.99

[a] CF = chloroform, CN = 1-chloronaphthalene, CB = chlorobenzene. [b] Average values over at least 4 devices.

Table S3. Optimization of the solar cell devices based on **SM3**.

Processing solvent[a]	**SM3**:$PC_{71}BM$	Total concentration (mg mL^{-1})	V_{OC} (V)	J_{SC} (mA cm^{-2})	FF	Average η (%)[b]	Best η (%)
CF	1:1	16	0.86	7.04	0.35	2.11	2.42
CF + 1% CN	1:1	16	0.85	6.41	0.32	1.73	1.83
CF + 3% CN	1:1	16	0.61	3.68	0.30	0.70	1.07

[a] CF = chloroform, CN = 1-chloronaphthalene. [b] Average values over at least 4 devices.

7. External quantum efficiency

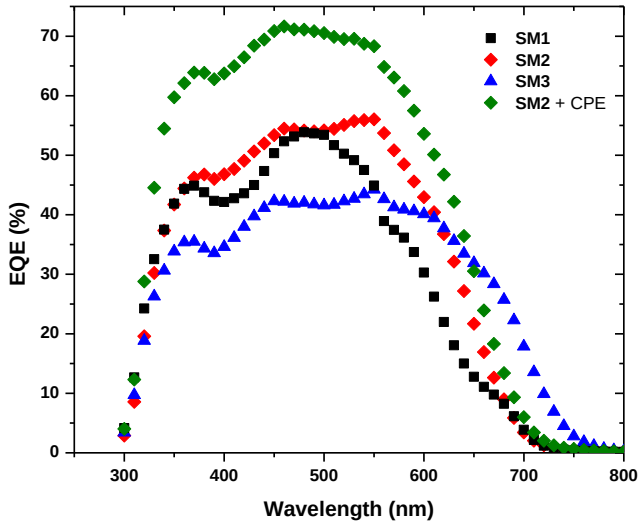

Figure S12. EQE spectra for average performing solar cell devices comprising **SM1**–**3**, processed from the optimal solvents. The **SM2** device employing the CPE interlayer is also portrayed. The current densities extracted from the EQE measurements performed on the best devices correlate with the measured J_{sc} values, in accordance with standard measurement deviations (J_{EQE} *vs* J_{sc}: 7.08 vs 6.51, 10.97 vs 10.79, 8.81 vs 9.13 and 7.95 vs 7.01 mA cm^{-2} for **SM1** in $CHCl_3$ +1% CN, **SM2** (in $CHCl_3$) with and without CPE interlayer, and **SM3** (in $CHCl_3$), respectively).

8. Conjugated polyelectrolyte structure

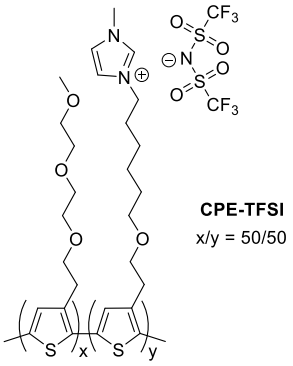

Figure S13. Chemical structure of the employed conjugated polyelectrolyte.[8]

9. Fourier transform photocurrent spectroscopy

FTPS spectra for small molecule organic solar cells based on **SM1–3** blended with $PC_{71}BM$ (fabricated using the optimized processing conditions, affording highest efficiencies, for each material combination) are shown in Fig. S14, together with the fits of Equation S1 to the charge transfer (CT) band.[9]

$$EQE_{PV}(E) = \frac{f}{E\sqrt{4\pi\lambda kT}} exp\left(\frac{-(E_{CT}+\lambda-E)^2}{4\lambda kT}\right) \qquad \text{(Eq. S1)}$$

Herein, *f* represents a term that describes the number of CT states, the internal quantum efficiency and the electronic coupling, E_{CT} is the energy of the CT state, λ is related to the width of the CT absorption band, *k* is the Boltzmann constant and *T* the temperature.

E_{CT} is significantly lower for the device based on **SM1** (E_{CT} = 1.29 eV) than for **SM2** (E_{CT} = 1.40 eV) and **SM3** (E_{CT} = 1.47 eV), which corresponds with the lower V_{OC} values observed (see Table 2). E_{CT} follows the trend of V_{OC} for the prepared devices.

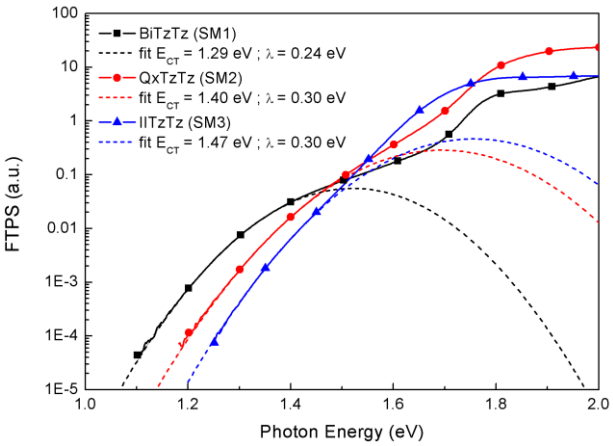

Figure S14. FTPS spectra of the CT region, with fits to Equation S1 (indicated by the dashed lines), for **SM1**–**3**:$PC_{71}BM$ small molecule organic solar cells (fabricated using the optimal processing conditions).

McGehee *et al.* recently showed that energetic disorder contributes to λ.[10] Their results indicated that when a system shows more specific polymer:fullerene conformations, λ lowers, which can be related to a decrease of the energetic distribution of CT states. In this work, focusing on small molecules rather than conjugated polymers, λ is lower for **SM1** (λ = 0.24 eV), which also exhibits the highest degree of crystallinity (according to the RHC analysis, see Fig. 2).

10. Charge carrier mobility data

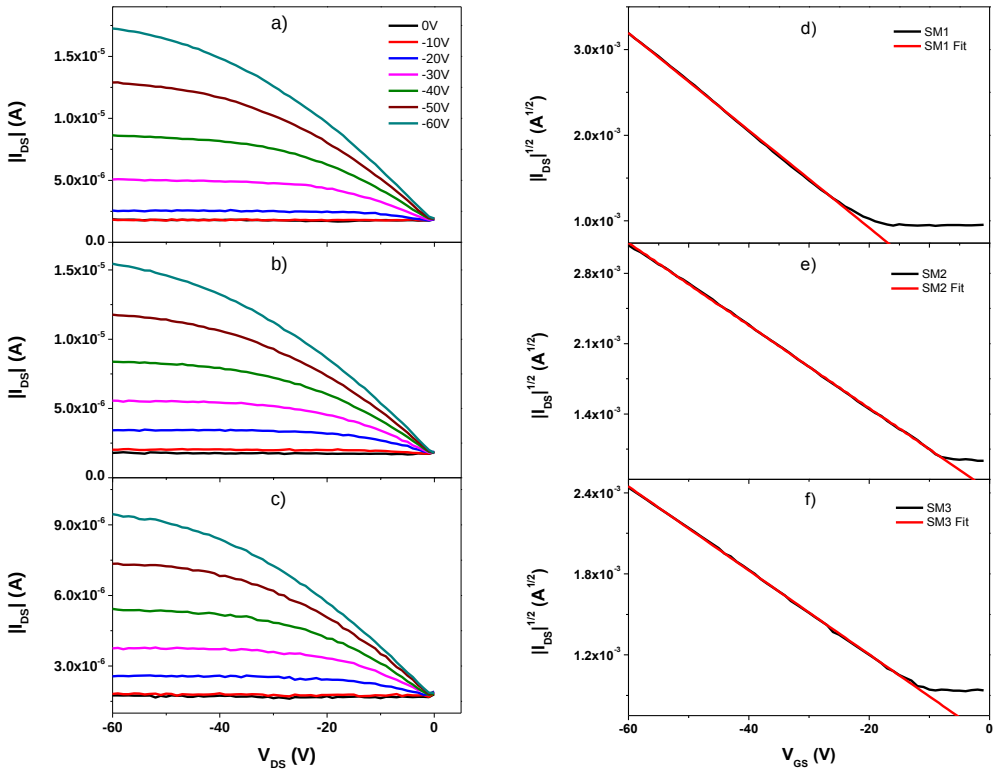

Figure S15. FET transfer and output curves of the transistors constructed with **SM1** (a, d), **SM2** (b, e) and **SM3** (c, f). The transfer characteristics were acquired in saturation regime at V_{DS} = −60 V. The red lines represent the fits used to extract the hole mobilities.

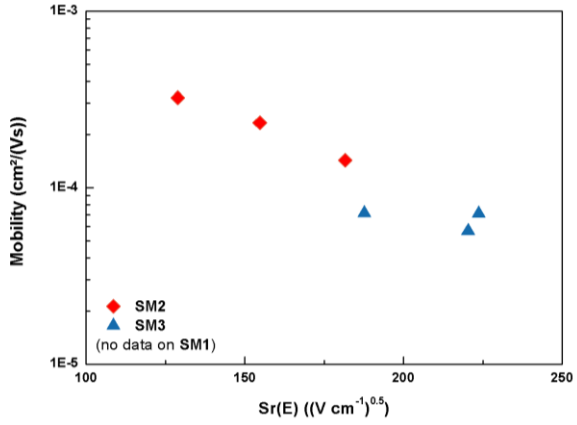

Figure S16. Data obtained from photo-CELIV measurements on organic solar cell devices based on **SM2–3** with photoactive layer thicknesses > 300 nm (no data could be acquired for **SM1**). Charge carrier mobilities of ~2 x 10^{-4} and ~6 x 10^{-5} cm^2 V^{-1} s^{-1} were acquired for the **SM2** and **SM3** devices, respectively, correlating with the observed J_{SC} trend.

11. References

(1) W.-Y. Wong, X.-Z. Wang, Z. He, K.-K. Chan, A. B. Djurišić, K.-Y. Cheung, C.-T. Yip, A. M.-C. Ng, Y.-Y. Xi, C. S.-K. Mak and W.-K. Chan, *J. Am. Chem. Soc.*, 2007, **129**, 14372.

(2) P. Verstappen, J. Kesters, W. Vanormelingen, G. H. L. Heintges, J. Drijkoningen, T. Vangerven, L. Marin, S. Koudjina, B. Champagne, J. Manca, L. Lutsen, D. Vanderzande and W. Maes, *J. Mater. Chem. A*, 2015, **3**, 2960.

(3) W. Wang, Z. Ma, Z. Zhang, K. Vandewal, P. Henriksson, O. Inganäs, F. Zhang and M. R. Andersson, *J. Am. Chem. Soc.*, 2011, **133**, 14244.

(4) (*a*) R. L. Danley, P. A. Caulfield and S. R. Aubuchon, *Am. Lab.*, 2008, **40**, 9; (*b*) T. Ghoos, N. Van den Brande, M. Defour, J. Brassinne, C.-A. Fustin, J.-F. Gohy, S. Hoeppener, U. S. Schubert, W. Vanormelingen, L. Lutsen, D. J. Vanderzande, B. Van Mele and W. Maes, *Eur. Polym. J.*, 2014, **53**, 206.

(5) (*a*) J. Bard and L. R. Faulkner, *Electrochemical methods: fundamentals and applications*, 2nd Ed., 2001, Wiley; (*b*) S. Trasatti, *Pure Appl. Chem.*, 1986, **58**, 95.

(6) D. Veldman, S. C. J. Meskers and R. A. J. Janssen, *Adv. Funct. Mater.*, 2009, **19**, 1939.

(7) K. Vandewal, L. Goris, I. Haeldermans, M. Nesládek, K. Haenen, P. Wagner and J. V. Manca, *Thin Solid Films*, 2008, **516**, 7135.

(8) (*a*) J. Kesters, T. Ghoos, H. Penxten, J. Drijkoningen, T. Vangerven, D. M. Lyons, B. Verreet, T. Aernouts, L. Lutsen, D. Vanderzande, J. Manca and W. Maes, *Adv. Energy Mater.*, 2013, **3**, 1180; (*b*) T. Ghoos, J. Brassinne, C.-A. Fustin, J.-F. Gohy, M. Defour, N. Van Den Brande, B. Van Mele, L. Lutsen, D. J. Vanderzande and W. Maes, *Polymer*, 2013, **54**, 6293; (*c*) W. Vanormelingen, J. Kesters, P. Verstappen, J. Drijkoningen, J. Kudrjasova, S. Koudjina, V. Liégeois, B. Champagne, J. Manca, L. Lutsen, D. Vanderzande and W. Maes, *J. Mater. Chem. A*, 2014, **2**, 7535.

(9) K. Vandewal, K. Tvingstedt, A. Gadisa, O. Inganäs and J. V. Manca, *Phys. Rev. B*, 2010, **81**, 125204.

(10) K. R. Graham, C. Cabanetos, J. P. Jahnke, M. N. Idso, A. El Labban, G. O. Ngongang Ndjawa, T. Heumueller, K. Vandewal, A. Salleo, B. F. Chmelka, A. Amassian, P. M. Beaujuge and M. D. McGehee, *J. Am. Chem. Soc.*, 2014, **136**, 9608.